

What is the Impact of 5G Towers on the Exposure over Children, Teenagers and Sensitive Buildings?

Luca Chiaraviglio,^(1,2) Chiara Lodovisi,^(1,2) Daniele Franci,⁽³⁾ Enrico Grillo,⁽³⁾ Settimio Pavoncello,⁽³⁾ Tommaso Aureli,⁽³⁾ Nicola Blefari-Melazzi,^(1,2) Mohamed-Slim Alouini,⁽⁴⁾

(1) EE Department, University of Rome Tor Vergata, Rome, Italy,

email {luca.chiaraviglio@uniroma2.it, Lodovisi@ing.uniroma2.it, blefari@uniroma2.it}

(2) Consorzio Nazionale Interuniversitario per le Telecomunicazioni, Parma, Italy

(3) Agenzia Regionale per la Protezione Ambientale del Lazio (ARPA Lazio), Rome, Italy,

{daniele.franci, enrico.grillo, settimio.pavoncello, tommaso.aureli}@arpalazio.it

(4) CEMSE Division, King Abdullah University of Science and Technology, Thuwal, Saudi Arabia

email slim.alouini@kaust.edu.sa

Abstract—The rolling-out of 5G antennas over the territory is a fundamental step to provide 5G connectivity. However, little efforts have been done so far on the exposure assessment from 5G cellular towers over young people and sensitive buildings like schools and medical centers. The goal of this article is therefore to explain why the 5G service strongly leverages the deployment of 5G antennas over cellular towers, how a tower installation hosting 5G antennas affects exposure over the territory, and at what extent children/teenagers, schools and medical centers are impacted by the exposure from 5G towers.

5G networks are being deployed in many countries of the world. Despite the potentials of this technology have not been completely unleashed, a central point of debate is how 5G influences Electro-Magnetic Field (EMF) exposure over the population, and whether such exposure patterns will substantially increase in the forthcoming years [1]. In this context, the assessment of the exposure levels generated by mobile networks over children and teenagers is gaining attention in the academic community (see e.g., [2], [3]), as young people will (probably) receive higher exposure levels throughout their lives compared to older people - who tended to live in an era where mobile networks were not so widespread as today. In addition, the exposure assessment over sensitive places, such as schools and medical centers, is central for monitoring aspects, e.g., to (possibly) limit the amount of unwanted exposure over specific groups like students and patients.

Currently, there is no scientific evidence that base station exposure adhering to international guidelines (such as the International Commission on Non-Ionizing Radiation Protection (ICNIRP) ones [4])

is harmful for health [5], [6]. Nevertheless, the assessment of EMF radiated by base stations over children, teenagers and sensitive places may be a key aspect for current (and future) epidemiological studies [7], aimed at studying possible (but still not proven at present time) correlations between the levels of 5G exposure and the emergence of long-term health diseases (such as cancers and tumors). Despite the literature about EMF exposure assessment from mobile base stations (including other Radio-Frequency (RF) sources) is already rather mature (see e.g., [8]–[10] for pre-5G studies and [11]–[15] for 5G ones), there is currently a lack of studies focusing on the exposure radiated by 5G outdoor base stations over children, teenagers, and sensitive places.

More concretely, Morelli *et al.* [16] evaluate the EMF levels over children and adults by considering user terminals (and not base stations) as sources of exposure. Bonato *et al.* [17] investigate the personal exposure from indoor access points. Personal pre-5G exposure over children is collected through exposimeters and thoroughly analyzed by Birks *et al.* [18]. Pre-5G exposure in sensitive places (school buildings) is measured by Ramirez-Vazquez *et al.* [19]. Gallastegi *et al.* [20] perform a thorough assessment of pre-5G exposure over different areas (including homes and schools). Eventually, pre-5G exposure in kinder-gardens is analyzed by Bhatt *et al.* [21]. Finally, 5G exposure measurements for different locations in South Korea are analyzed by Selmaoui *et al.* [15]. Despite we recognize the importance of such previous works, none of them is tailored to the assessment of 5G exposure

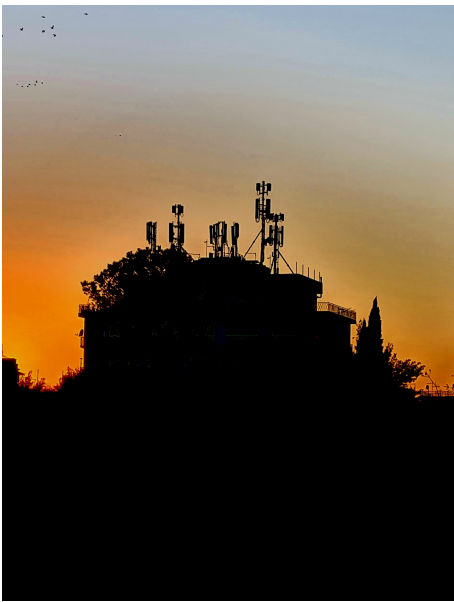


Fig. 1. Roof-top installation in the city of Rome encompassing different operators, sectors and antennas (including 5G ones).

from outdoor base stations over children, teenagers and sensitive areas - due to a different goal (e.g., personal devices rather than base stations), and/or a different focus (i.e., generic exposure assessment not tailored to children/teenagers and sensitive buildings), and/or a lack of exposure information about 5G (outdoor) base stations over the considered scenarios.

Our work goes one step further with respect to the literature, by shedding light on the exposure levels radiated by outdoor base stations (including 5G ones) over young people and sensitive places. We tackle this interesting problem by designing and evaluating a solid exposure assessment over realistic scenarios and conservative settings. Our work links together children and teenager data taken from national census, real positioning of the buildings (including the sensitive ones), real positioning of 5G (and pre-5G) base stations over the territory, realistic radio configurations and a conservative computation of exposure from each base station - including equipment operating on mm-Wave frequencies. In addition, we evaluate the exposure trends over the coming years, by integrating in our analysis the impact of 5G deployment level (i.e., from an early deployment up to maturity).

A key point of this article is the focus on the exposure levels radiated by 5G towers, i.e., base stations installed on self poles - a.k.a. “raw-land” - and roof-top installations, like the one shown

in Fig. 1. We intentionally leave apart from our analysis the radiation from small cells - a.k.a. micro installations -, whose exposure levels would be additive with respect to the ones radiated by 5G towers and considered in this work. Therefore, a natural question is: Why do we concentrate on 5G towers? To answer this question, we first present a brief overview on how 5G is currently implemented in commercial networks and the role of towers on the 5G deployment. We then analyse the root causes to explain why towers hosting 5G antennas are relevant for the assessment of 5G exposure. Finally, we present the results of our exposure analysis over children, teenagers and sensitive places. The work is complemented by an Appendix providing more technical details - which may be useful e.g., for the experts working in the field.

I. HOW IS 5G IMPLEMENTED IN COMMERCIAL NETWORKS?

The provisioning of the 5G service requires (obviously) the installation of (new) antennas over the territory. Each antenna is placed on a physical medium, which can be either a stand-alone pole for tower installations (roof-top or raw-land), or alternatively a wall/lighting pole (particularly for small cell deployments). In many countries in the world - such as Italy for example - the tower installation is currently the preferred option for deploying 5G networks, due to different reasons. First, cellular operators can reuse the existing towers - currently hosting pre-5G equipment - to install 5G antennas. In this way, the authorization steps for the installation of 5G antennas may be simplified and/or shortened in time. In addition, this choice tends to reduce the installation costs that are faced by operators compared to the design of a new site from the scratch - since electricity and wired connections required by 5G antennas are already available on the existing site. Moreover, small cells are not pervasively installed over the entire territory - being such option profitable only for those locations that provide an adequate return on investment. In particular, small base stations are instrumental to boost network capacity in shopping malls, conference centers, airports, train stations and stadium - where the mobile traffic is intense due to the simultaneous presence of thousands of terminals demanding wireless services in a very limited area.

On the contrary, the tower installation tends to be the most profitable option to serve wide areas in rural zones and entire portions of neighborhoods in urban deployments, with the ultimate goal of providing ubiquitous wireless coverage over the territory.

Having understood that towers are a fundamental way to realize 5G networks, we provide hereafter more technical details about the implementation of the 5G service in practice. A key driver to speed-up the 5G network deployment is the exploitation of the already installed 4G architecture. More concretely, 5G is often realized through the Non-StandAlone (NSA) configuration option [22], which allows running 5G network in conjunction (and not in parallel) with 4G. In this way, the 4G network is used to spread control signals (that are instrumental for example to select the base station serving a 5G user terminal), as well as to run the inner functionalities on the 4G network core. In the long term, 5G will be realized through the StandAlone (SA) option [22] - taking full control over wireless signals and network core functionalities. To this aim, many countries and single operators in the world have announced detailed plans for adopting 5G SA networks [23]. However, 4G networks will be still in operation even when the majority of connections will be realized through 5G - in order to guarantee legacy services. Therefore, the contribution of 4G antennas on the level of exposure can not be neglected - also to understand the exposure contribution of 5G with respect to pre-5G sources.

II. WHY ARE 5G TOWERS RELEVANT FOR THE ASSESSMENT OF THE EXPOSURE?

A tower installation typically hosts multiple antenna panels. State-of-the-art solutions for deploying 5G (and pre-5G) services include multiple-band antenna (see e.g., [24]), supporting sub-GHz 5G frequencies, as well as most of frequencies in use by pre-5G technologies (4G and even 2G). In addition, dedicated antennas are used to deploy 5G over higher frequencies, such as mid-band [25] and mm-Wave. The number of radiating sources in each antenna is not marginal, as 5G panels operating on mid-band and mm-Wave are composed of multiple radiating elements to realize Massive-multiple-input multiple-output (MIMO) and beamforming functionalities. This number is then increased when

the tower hosts multiple physical operators - each of them managing a set of antennas on the site. Therefore, the composite power radiated by all antennas of the tower is not negligible, especially in its surroundings - where most of radiation tends to concentrate.

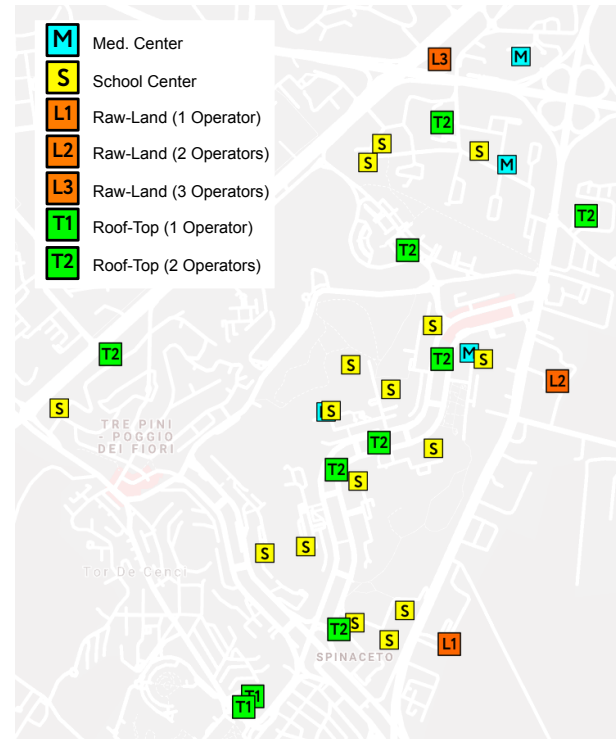
In this context, the assessment of the EMF radiated by a cellular tower is a fundamental (yet challenging) step. When considering urban zones, roof-top or raw-land towers are commonly installed in proximity to residential buildings, as well as sensitive ones. Clearly, the tower radiation level over its surroundings strongly depends on multiple aspects, including: *i*) the characteristics of the antennas installed on the tower (in terms, e.g., of adopted frequency, maximum radiated power, maximum gain, radiation diagram, horizontal orientation, mechanical/electrical tilting), *ii*) the relative 3D distance of the EMF evaluation point with respect to the considered tower and *iii*) attenuation effects introduced e.g., by walls and obstacles between the evaluation point and the tower.

The exposure assessment is further complicated when considering 5G antennas operating in the mid-band and mm-Wave frequencies, as such equipment implement smart antenna management features to realize the already mentioned massive-MIMO and beamforming features - generally resulting in different exposure levels compared to pre-5G equipment (see e.g., [12]). More in depth, the output power of a 5G antenna is split among multiple elements of the antenna panel, which are used to synthesize control and traffic beams over different locations of the territory. As a consequence, assuming that the whole amount of power radiated by the antenna panel is directed towards a single location of the territory is not realistic in practice, and proper power scaling factors have to be applied for a meaningful assessment of the EMF exposure [26].

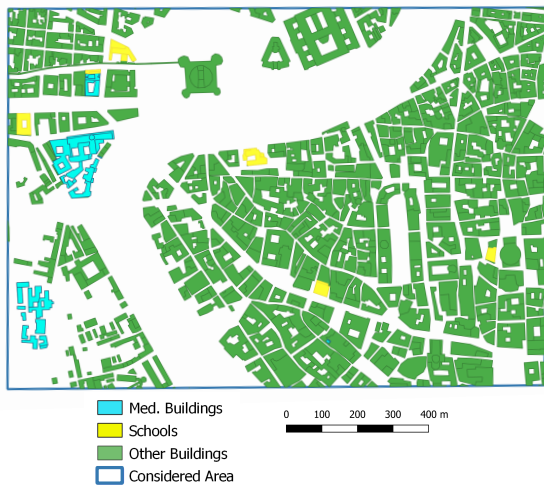
Interestingly, large scaling factors are applied to mid-band/mm-Wave antennas covering areas dense of buildings (e.g., urban zones) compared to ones serving sparse sets of houses (e.g., rural territory) [26], [27]. As a consequence, the exposure from a single tower may be potentially lower in a dense area compared to a sparse one. Intuitively, in fact, the beams in dense areas are more uniformly distributed over the territory compared to sparse zones, in which instead most of the beams are focused on specific locations (e.g., the few locations with



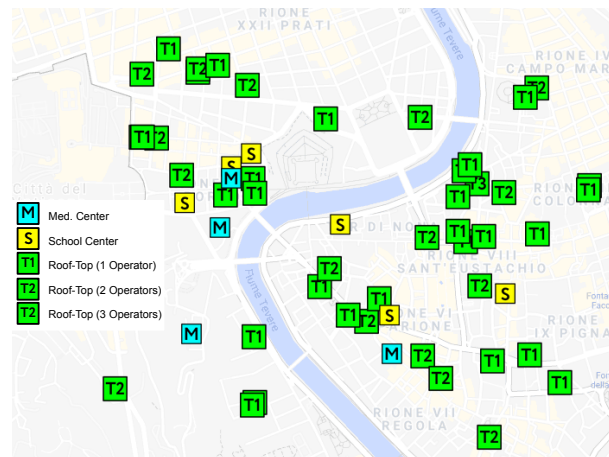
(a) Buildings and considered area - Spinaceto.



(b) Positioning of the sensitive places and cellular towers - Spinaceto.



(c) Buildings and considered area - Ponte-Parione.



(d) Positioning of the sensitive places and cellular towers - Ponte-Parione.

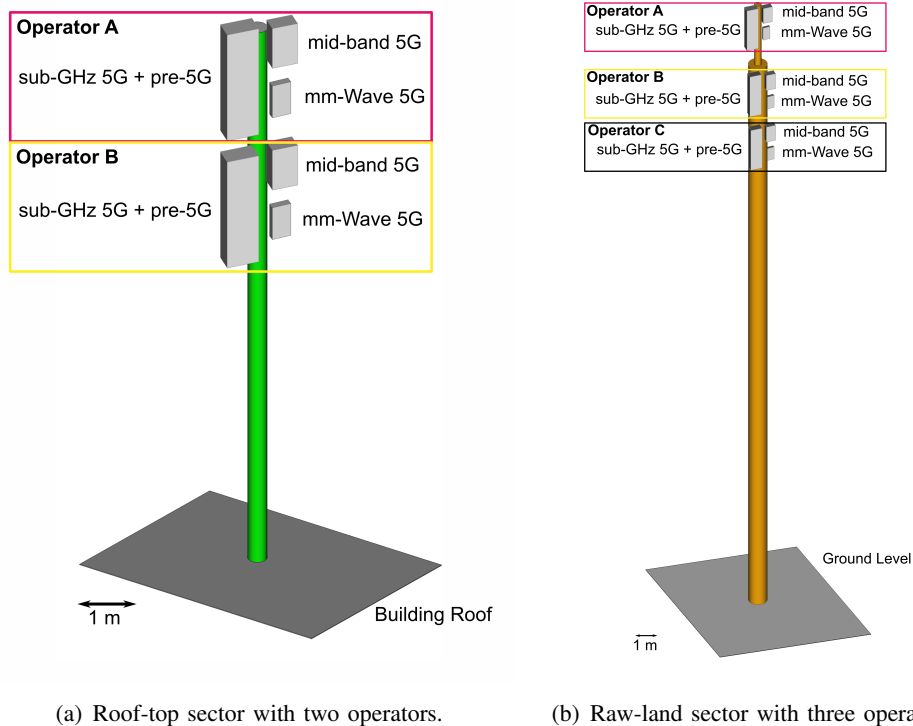
Fig. 2. Towers, buildings and sensitive locations in the considered scenarios (sub-figures best viewed in colors).

buildings), which therefore may receive an higher amount of exposure with respect to the dense case. However, the composite exposure depends also on the tower density, i.e., the number of towers simultaneously covering the same area of territory. In a dense area, the tower density is naturally higher compared to a sparse one (mainly due to higher capacity requirements), thus potentially increasing the total exposure that is radiated by multiple towers

covering the same location [28].

III. WHICH IS THE IMPACT OF 5G TOWERS ON THE EXPOSURE LEVELS?

Up to this point, we have understood that exposure from 5G towers strongly depends on the considered scenario. In the following, therefore, we present a sound exposure assessment performed over two representative areas in the city of Rome, by



(a) Roof-top sector with two operators.

(b) Raw-land sector with three operators.

Fig. 3. Antenna panel installations for each operator (example with one sector per operator): roof-top tower (left) vs. raw-land tower (right).

considering a dense neighborhood in the historical-center (called Ponte-Parione) and a sparse one (called Spinaceto). We believe that such scenarios are able to capture multiple aspects that strongly affect the exposure levels, including different 5G power scaling factors (which depend, e.g., on the sparse vs. dense building distribution), as well as different tower densities. The whole description of the input data and the methodology is detailed in the Appendix, while here we concentrate on the main outcomes.

The real positioning of buildings (including schools and medical centers) and cellular towers is reported in Fig. 2. More in depth, we have included in our analysis all the towers that are located inside the considered area, as well as all the outer ones that are installed within 300 m from the area border - in order to avoid a potential exposure underestimation on the borders. Several considerations hold by analyzing the subfigures Fig. 2(a)-2(d). First, the building density in Fig. 2(a),2(c) is clearly higher in Ponte-Parione compared to Spinaceto: this is due to the fact that the former mainly includes historical buildings closely placed to each other, while the latter is a newer neighborhood, typically composed of spatially-distanced buildings - including large green areas without any building. Second,

both scenarios include sensitive centers (schools and medical centers), which are spread over the considered territory. Third, each school/medical center is normally composed of different buildings (adjacent to each other), as shown by yellow and cyan colors in Fig.2(a),2(c). Fourth, the towers are rather spread over Ponte-Parione territory (Fig. 2(d)), while in Spinaceto the towers tend to be mainly placed in proximity to the buildings (Fig. 2(b)). Fifth, the roof-top installation is the preferred option for Spinaceto - which however hosts some raw-land towers. On the contrary, Ponte-Parione does not include any raw-land, mainly due to the fact that such tower type generally requires to find ground locations without any buildings in the close surroundings - a hard goal to pursue in Ponte-Parione. Sixth, many towers are located close to the sensitive buildings (Fig. 2(b),2(d)). Seventh, the majority of installations in Spinaceto host at least two distinct operators on the same tower, while the option with a single operator per tower is the most used in Ponte-Parione.

Apart from the number of operators per tower, we have also collected sector information for each installation (including the number of sectors and the sector orientation). We have then designed two panel installations for each sector and each type

of tower in the scenario, as shown in Fig. 3 for a representative example with one sector. More in depth, we have assumed that each sector of each operator is composed of three distinct antenna panels: a quadri-band panel (used for sub-GHz 5G and 2G/4G frequencies), a mid-band panel (used for 5G frequencies operating in the 3.6-3.8 GHz range) and a mm-Wave panel (used for 5G frequencies in the range 26.5-27.5 GHz). By adopting a uniform panel design across all operators, we are able to make a fair analysis, namely: *i*) all operators offer similar 5G connectivity options over the scenarios, and *ii*) all frequencies currently allocated to 5G in Italy are used. The features of each panel in terms of tilting/power/gain/radiation diagram are taken from real equipment and realistic configurations, which in turn depend on the tower type (details in the Appendix).

Eventually, Fig. 3(a) reports (in scale) the positioning of two operators for the roof-top installation, while Fig. 3(b) highlights the positioning of three operators (again in scale) for a raw-land installation. In both cases, the antenna panels of different operators are vertically stacked (rather than horizontally stacked). The adoption of a vertical alignment rather than an horizontal one (in which all panels are placed on the pole summit) introduces multiple advantages, namely: *i*) a conservative evaluation of exposure, since the panels tend to be placed at a lower altitude (when multiple operators are hosted), and *ii*) a uniform tower design across all installation sites, as each tower is always composed of a single pole (while with an horizontal alignment other supporting poles might be needed - depending on the number of operators hosted by the tower).

We then compute the EMF levels over all the buildings in the considered scenarios, by following the methodology reported in the Appendix. Unless otherwise specified, the EMF assessment is based on a set of conservative (and worst-case) assumptions, which include: *i*) EMF evaluated on the building roof level, *ii*) free-space propagation conditions, *iii*) no building attenuation, *iv*) pre-5G antennas and sub-GHz 5G antennas radiating at the maximum power (corresponding to the maximum traffic condition), *v*) mid-band and mm-Wave 5G power scaling factors depending on the building distribution (sparse vs. dense) and the level of 5G adoption (i.e., from early deployment to maturity). The building exposure value is then assigned to the

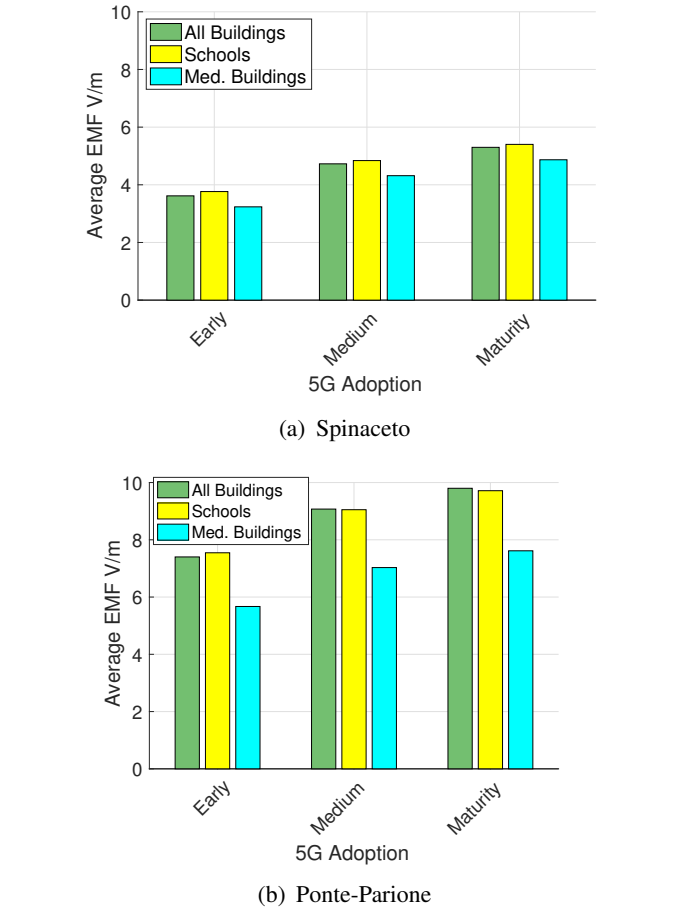


Fig. 4. Average EMF values of the building exposure vs. level of 5G adoption (sub-figures best viewed in colors).

children and teenagers living in that building (based on census information). In addition, the exposure of schools and medical centers is extracted from the set of buildings.

We then move our attention on the analysis of the obtained results. Fig. 4 reports the average EMF over the buildings, by differentiating between the building type and the level of 5G adoption. Intuitively, the power radiated by mid-band/mm-Wave 5G antennas is proportional to the adoption level, and therefore the exposure tends to (obviously) increase when passing from an early level to the maturity one.

The figure then further differentiates between Spinaceto (Fig. 4(a)) and Ponte-Parione (Fig. 4(b)). Several considerations hold by comparing Fig. 4(a)-4(b). First, the exposure over schools is rather similar to the one received by the whole set of buildings in both scenarios. On the contrary, medical buildings receive a lower exposure compared to the other building categories. Second, the expo-

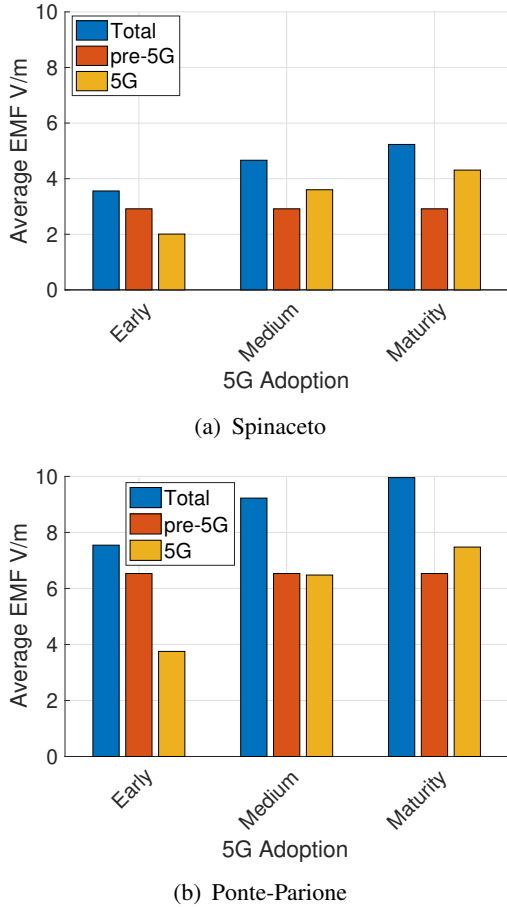


Fig. 5. Impact of the 5G adoption level on the average exposure over children and teenagers (sub-figures best viewed in colors).

sure tends to increase when passing from early to maturity levels of 5G adoption - in all scenarios (as expected). However, the maximum exposure increase is typically lower than 2 V/m and 3 V/m for Spinaceto and Ponte-Parione, respectively. Fourth, the buildings in Ponte-Parione receive an higher average exposure than the ones in Spinaceto, for all 5G adoption levels. This trend may be explained by the higher tower density in Ponte-Parione compared to Spinaceto. Therefore, despite the 5G radiated power per tower is lower in Ponte-Parione than in Spinaceto, the composite exposure from all towers is higher in the former compared to the latter.

In the following step, we focus on the different exposure components, by considering the average exposure that is received over children and teenagers living in the two areas. To this aim, Fig. 5 differentiates between: *i*) pre-5G exposure, *ii*) 5G exposure, *iii*) whole exposure (5G + pre-5G). The analysis is then repeated for the different adoption levels of 5G (from early level to maturity one). Interestingly,

the contribution of 5G is lower than the pre-5G one for the early 5G adoption case. This outcome corresponds to the current situation, in which 5G represents a fraction of the exposure generated by pre-5G antennas (mainly 4G and 2G) [13]. Then, when passing from early to medium adoption level, the contribution of 5G exposure tends to increase - as a consequence of the radiated power growth by mid-band and mm-Wave antennas. At last, the exposure from 5G becomes higher than the pre-5G one. This event occurs when a medium adoption level is achieved in Spinaceto (Fig. 5(a)) and only when a maturity level is reached by Ponte-Parione (Fig. 5(b)). Intuitively, in fact, the different power scaling factors applied in the two scenarios (resulting from the different spatial distribution of the beams) determine the share of 5G exposure with respect to the pre-5G one.

Up to this point, we have considered the average exposure level, without analyzing the exposure variations of the single samples in each group (children/teenagers, schools and medical buildings). To shed light on this issue, Fig. 6 reports the EMF exposure vs. the percentage of children/teenagers, school buildings and medical buildings over the two scenarios. Each curve can be analyzed in this way: given a percentage value, the corresponding EMF value read on the curve is the maximum exposure that is achieved with that percentage. Clearly, when the percentage equals 100%, the EMF value read on the curve is the maximum EMF exposure over all the samples. The slope of the curve captures the EMF exposure variation over the samples: when the curve is almost vertical, the variation is low; when the curve is more horizontal, the variation is increased. Each curve in the subfigures then highlights the following EMF metrics: *i*) pre-5G exposure (continuous line), *ii*) 5G exposure - early adoption (dashed line), *iii*) 5G exposure - medium adoption (dashed-dotted line), *iv*) 5G exposure - maturity adoption (dotted line).

Several considerations hold by observing Fig. 6(a)-Fig. 6(f). First of all, the curves capturing the exposure over children and teenagers are smoother compared to the ones of schools and medical buildings. This is due to the fact that children and teenagers are rather spread over the buildings in the considered scenarios, while on the contrary schools and medical centers represent a small fraction of the total buildings. As a result,

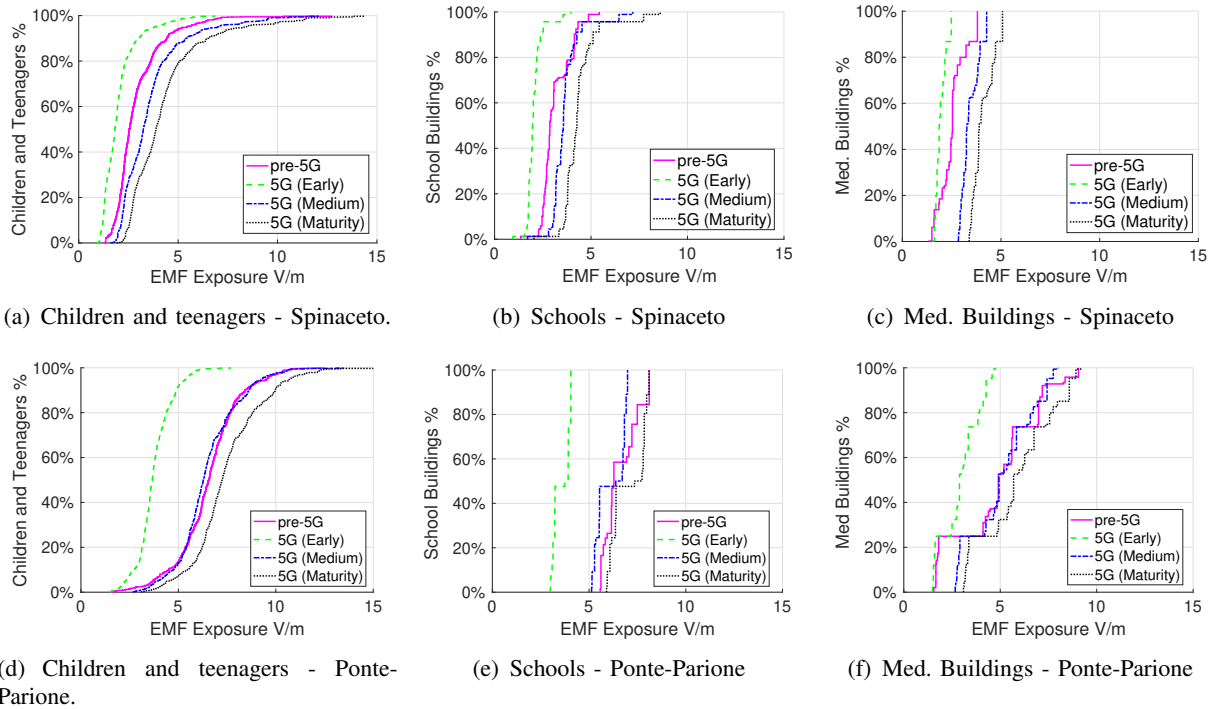


Fig. 6. Percentage of children and teenagers (left), schools (center) and med. buildings (right) vs. EMF exposure.

the number of samples is larger for the formers and smaller for the latter, and thus resulting in smooth lines. Second, EMF exposure due to 5G (early adoption) is lower than pre-5G one for all percentages of children/teenagers (Fig. 6(a),6(d)) and school buildings (Fig. 6(b),6(e)). In practical words, a child/teenager or a school building always receives an higher amount of exposure from pre-5G antennas than 5G ones during the early 5G adoption level. Third, the evolution of 5G adoption towards maturity results in larger EMF exposure levels by 5G compared to pre-5G ones for children/teenagers and sensitive places, in both scenarios. Fifth, the maximum 5G exposure is lower than 15 V/m for children and teenagers, while always lower than 10 V/m for schools and medical buildings - well below maximum EMF exposure limits defined by ICNIRP for the general public over the considered frequencies [4].¹ Sixth, the exposure in Ponte-Parione tends to be higher than Spinaceto for almost all the samples when considering the medium and maturity 5G adoption cases, due again to the higher tower density of the former with respect to the latter.

In the final part of our analysis, we investigate

¹We have also verified that the composite exposure of 5G and pre-5G adheres to the EMF limits (details in the Appendix).

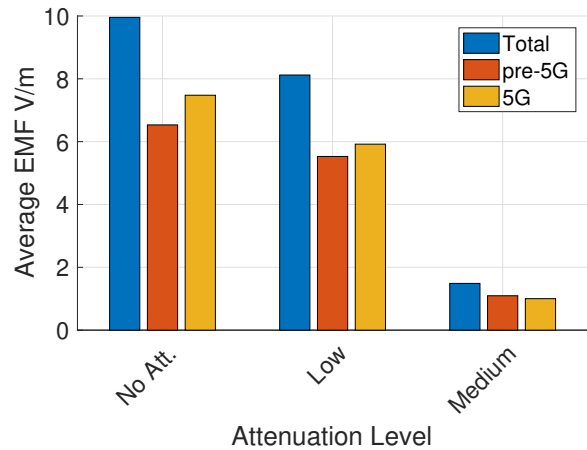


Fig. 7. Impact of introducing the building attenuation on the EMF exposure over children and teenagers (Ponte-Parione scenario - 5G maturity setting).

the impact of including different attenuation levels on the EMF assessment over children and teenagers. More in depth, we exploit the attenuation model defined in the International Telecommunication Union (ITU) recommendation P.2109-1 [29] to compute the attenuation values. Clearly, computing the exact attenuation values for each child/teenager is a very challenging task. In particular, the attenuation level depends on multiple building features (such as building materials, walls thickness, windows/-

doors type and positioning, glass type, etc.), as well as the positioning of children/teenagers inside the building (e.g., proximity vs. farness with respect to the windows), which are (obviously) not under our control. Therefore, rather than targeting the exact computation of the attenuation for each child/teenager, we consider two representative cases, namely: *i*) low attenuation level (computed with the ITU model by setting 1% of probability) and *ii*) medium attenuation level (computed by averaging the attenuation values retrieved from the ITU model between 1% and 99% of probability).

Fig. 7 shows the EMF exposure over children and teenagers in Ponte-Parione (with 5G maturity setting), by also including the case without attenuation for comparison. As expected, the attenuation level has a large impact on the received exposure over children and teenagers, resulting in a notable exposure decrease for the medium setting compared to the other cases. In addition, the attenuation strongly affects the relative share of 5G exposure with respect to pre-5G one. Without attenuation, in fact, 5G exposure is higher than pre-5G one. When attenuation is introduced, the share of 5G exposure with respect to pre-5G one is reduced, and eventually the exposure from 5G becomes lower than the pre-5G one when a medium attenuation is assumed. This effect is expected, as 5G includes mid-band and mm-Wave frequencies, which are higher than the ones in use by pre-5G, and are therefore subject to larger propagation losses.

IV. SUMMARY AND FUTURE WORK

We have assessed the impact of 5G towers on the EMF exposure over children/teenagers, school buildings and medical buildings over two realistic scenarios. Our results reveal that, although 5G exposure radiated by towers is initially lower than the pre-5G one, 5G will become the dominant source of exposure from cellular towers when a maturity level will be reached. However, the scaling factors applied to the maximum power radiated by mid-band/mm-Wave antennas, the tower distribution and the positioning of the buildings are important aspects heavily influencing the exposure levels over young people and sensitive places. Eventually, the actual level of exposure over children and teenagers is largely impacted by the building attenuation level, which has a stronger effect over mid-band and mm-Wave 5G frequencies compared to pre-5G ones.

As future works, we plan to extend our assessment to whole municipalities/cities, including zones covered by small cells. In addition, as propagation has a strong effect over the exposure received by children and teenagers, massive campaigns of EMF measurements from 5G towers should be performed, especially inside the buildings. Finally, the joint assessment of 5G exposure from both towers and other installations - such as intelligent reflecting surfaces and distributed antenna systems - is another interesting step. This activity will also include the exposure trends analysis of pre-5G sources.

REFERENCES

- [1] M. A. Jamshed, F. Heliot, and T. W. Brown, "A survey on electromagnetic risk assessment and evaluation mechanism for future wireless communication systems," *IEEE Journal of Electromagnetics, RF and Microwaves in Medicine and Biology*, vol. 4, no. 1, pp. 24–36, 2019.
- [2] J.-H. Moon, "Health effects of electromagnetic fields on children," *Clinical and experimental pediatrics*, vol. 63, no. 11, p. 422, 2020.
- [3] L. E. Birks, L. van Wel, I. Liorni, L. Pierotti, M. Guxens, A. Huss, M. Foerster, M. Capstick, M. Eeftens, H. El Marroun, M. Estarlich, M. Gallastegi, L. G. Safont, W. Joseph, L. Santa-Marina, A. Thielens, M. Torrent, T. Vrijkotte, J. Wiart, M. Rössli, E. Cardis, R. Vermeulen, and M. Vrijheid, "Radiofrequency electromagnetic fields from mobile communication: Description of modeled dose in brain regions and the body in European children and adolescents," *Environmental Research*, vol. 193, p. 110505, 2021.
- [4] International Commission on Non-Ionizing Radiation Protection (ICNIRP), "ICNIRP guidelines on limiting exposure to time-varying electric, magnetic and electromagnetic fields (100 kHz to 300 GHz)." Available at: <https://www.icnirp.org/cms/upload/publications/ICNIRPrfgdl2020.pdf>, Jul. 2020. Last Accessed: 29th Sept. 2020.
- [5] J. Bushberg, C. Chou, K. Foster, R. Kavet, D. Maxson, R. Tell, and M. Ziskin, "IEEE Committee on Man and Radiation - COMAR Technical Information Statement: Health and safety issues concerning exposure of the general public to electromagnetic energy from 5G wireless communications networks," *Health Physics*, vol. 119, no. 2, p. 236, 2020.
- [6] L. Chiaraviglio, A. Elzanaty, and M.-S. Alouini, "Health Risks Associated with 5G Exposure: A View from the Communications Engineering Perspective," *IEEE Open Journal of the Communications Society*, vol. 2, pp. 1–45, 2021.
- [7] K. Karipidis, R. Mate, D. Urban, R. Tinker, and A. Wood, "5G mobile networks and health - a state-of-the-science review of the research into low-level RF fields above 6 GHz," *Journal of Exposure Science & Environmental Epidemiology*, pp. 1–21, 2021.
- [8] P. Gajšek, P. Ravazzani, J. Wiart, J. Grellier, T. Samaras, and G. Thuróczy, "Electromagnetic field exposure assessment in Europe radiofrequency fields (10 MHz–6 GHz)," *Journal of exposure science and environmental epidemiology*, vol. 25, no. 1, p. 37, 2015.
- [9] S. Sagar, S. Dongus, A. Schoeni, K. Roser, M. Eeftens, B. Struchen, M. Foerster, N. Meier, S. Adem, and M. Rössli, "Radiofrequency electromagnetic field exposure in everyday microenvironments in Europe: A systematic literature review,"

- Journal of Exposure Science and Environmental Epidemiology*, vol. 28, no. 2, p. 147, 2018.
- [10] Y. Boussad, X. Chen, A. Legout, A. Chaintreau, and W. Dabous, *Longitudinal Study of Exposure to Radio Frequencies at Population Scale*. PhD thesis, Inria & Université Nice Sophia Antipolis, CNRS, I3S, Sophia Antipolis . . . , 2021.
- [11] D. Colombi, P. Joshi, B. Xu, F. Ghasemifard, V. Narasaraju, and C. Törnevik, “Analysis of the actual power and EMF exposure from base stations in a commercial 5G network,” *Applied Sciences*, vol. 10, no. 15, p. 5280, 2020.
- [12] S. Adda, T. Aureli, S. D’elia, D. Franci, E. Grillo, M. D. Migliore, S. Pavoncello, F. Schettino, and R. Suman, “A theoretical and experimental investigation on the measurement of the electromagnetic field level radiated by 5g base stations,” *IEEE Access*, vol. 8, pp. 101448–101463, 2020.
- [13] L. Chiaraviglio, C. Lodovisi, D. Franci, S. Pavoncello, T. Aureli, N. Blefari-Melazzi, and M.-S. Alouini, “Massive measurements of 5g exposure in a town: Methodology and results,” *IEEE Open Journal of the Communications Society*, vol. 2, pp. 2029–2048, 2021.
- [14] S. Aerts, K. Deprez, D. Colombi, M. Van den Bossche, L. Verloock, L. Martens, C. Tornevik, and W. Joseph, “Assessment of 5G NR base station RF-EMF exposure in a commercial network in Switzerland,” in *Joint Annual Meeting of the Bioelectromagnetics Society and the European BioElectromagnetics Association (BioEM 2021)*, pp. 17–22, 2021.
- [15] B. Selmaoui, P. Mazet, P.-B. Petit, K. Kim, D. Choi, and R. de Seze, “Exposure of the South Korean population to the 5th generation (5G) of mobile phone networks (3.4 to 3.8 GHz) and its respective contribution among other radio frequencies in the country,” in *2021 XXXIVth General Assembly and Scientific Symposium of the International Union of Radio Science (URSI GASS)*, pp. 1–4, IEEE, 2021.
- [16] M. S. Morelli, S. Gallucci, B. Siervo, and V. Hartwig, “Numerical Analysis of Electromagnetic Field Exposure from 5G Mobile Communications at 28 GHz in Adults and Children Users for Real-World Exposure Scenarios,” *International Journal of Environmental Research and Public Health*, vol. 18, no. 3, p. 1073, 2021.
- [17] M. Bonato, L. Dossi, E. Chiaramello, S. Fiocchi, S. Gallucci, G. Tognola, P. Ravazzani, and M. Parazzini, “Human RF-EMF exposure assessment due to access point in incoming 5G indoor scenario,” *IEEE Journal of Electromagnetics, RF and Microwaves in Medicine and Biology*, 2020.
- [18] L. E. Birks, B. Struchen, M. Eeftens, L. van Wel, A. Huss, P. Gajšek, L. Kheifets, M. Gallastegi, A. Dalmau-Bueno, M. Estarlich, M. F. Fernandez, I. K. Meder, A. Ferrero, A. Jimenez-Zabala, M. Torrent, T. G. Vrijkotte, E. Cardis, J. Olsen, B. Valic, R. Vermeulen, M. Vrijheid, M. Rössli, and M. Guxens, “Spatial and temporal variability of personal environmental exposure to radio frequency electromagnetic fields in children in Europe,” *Environment international*, vol. 117, pp. 204–214, 2018.
- [19] R. Ramirez-Vazquez, I. Escobar, A. Thielens, and E. Arribas, “Measurements and analysis of personal exposure to radiofrequency electromagnetic fields at outdoor and indoor school buildings: a case study at a spanish school,” *IEEE Access*, vol. 8, pp. 195692–195702, 2020.
- [20] M. Gallastegi, A. Huss, L. Santa-Marina, J. J. Aurrekoetxea, M. Guxens, L. E. Birks, J. Ibarluzea, D. Guerra, M. Rössli, and A. Jiménez-Zabala, “Children’s exposure assessment of radiofrequency fields: Comparison between spot and personal measurements,” *Environment international*, vol. 118, pp. 60–69, 2018.
- [21] C. R. Bhatt, M. Redmayne, B. Billah, M. J. Abramson, and G. Benke, “Radiofrequency-electromagnetic field exposures in kindergarten children,” *Journal of exposure science & environmental epidemiology*, vol. 27, no. 5, pp. 497–504, 2017.
- [22] *3GPP TR 21.915 V15.0.0 (2019-09) Release 15 Description*. Available at <https://portal.3gpp.org/desktopmodules/Specifications/SpecificationDetails.aspx?specificationId=3389>, last accessed on 12th Jan. 2022.
- [23] *5G Standalone 2021 – Summary*. Available at <https://gsacom.com/paper/5g-standalone-2021-summary/>, last accessed on 18th September 2020.
- [24] *Commscope 12-port sector antenna RRZZVV-65B-R6H4*. Available at <https://www.commscope.com/globalassets/digizuite/263290-p360-rrzzvv-65b-r6h4-comprehensiveexternal.pdf>, last accessed on 4th Jan. 2022.
- [25] *Ericsson Antenna Integrated Radio (AIR) for mid-band 5G*. Available at <https://www.ericsson.com/en/newsroom/photo-library/network-products>, last accessed on 4th Jan. 2022.
- [26] *IEC TR 62669 – Edition 2.0 2019/04 - Case Studies supporting IEC 62232 – Determination of RF field strength, power density and SAR in the vicinity of radiocommunications base stations for the purpose of evaluating human exposure*. Available at <https://webstore.iec.ch/publication/62014>, last accessed on 12th Jan. 2022.
- [27] B. Thors, A. Furuskär, D. Colombi, and C. Törnevik, “Time-Averaged Realistic Maximum Power Levels for the Assessment of Radio Frequency Exposure for 5G Radio Base Stations Using Massive MIMO,” *IEEE Access*, vol. 5, pp. 19711–19719, 2017.
- [28] L. Chiaraviglio, S. Turco, G. Bianchi, and N. Blefari-Melazzi, “Cellular Network Densification Increases Radio-Frequency Pollution: True or False?,” *IEEE Transactions on Wireless Communications*, 2021.
- [29] *ITU-R P.2109-1 Prediction of building entry loss*. Available at https://www.itu.int/dms_pubrec/itu-r/rec/p/R-REC-P.2109-1-201908-I!!PDF-E.pdf, last accessed on 4th Jan. 2022.

APPENDIX A

METHODOLOGY AND ADDITIONAL RESULTS

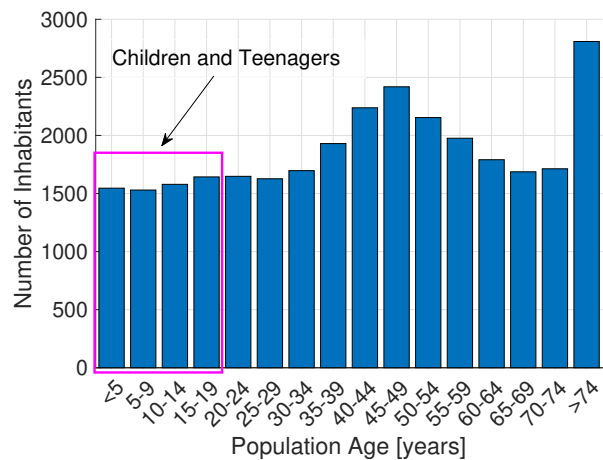
We provide hereafter more insights about the following aspects: *i*) collection of buildings and population data, *ii*) collection of tower data, *iii*) exposure assessment procedure, *iv*) description of the methodology to generate Fig. 4-7. Finally, the Appendix is complemented by a set of additional results.

A. Buildings and Population Data

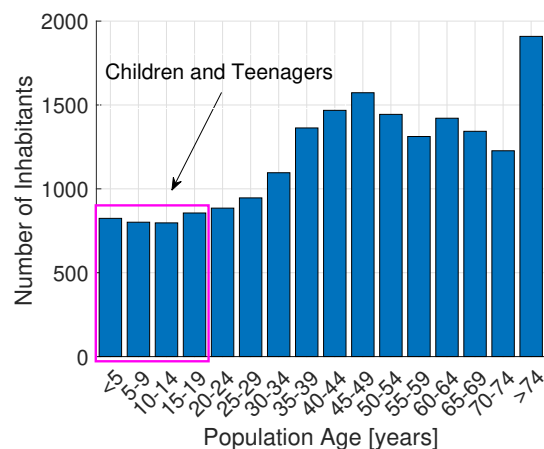
Obtaining reliable information about buildings and population in the considered areas is a fundamental step for the meaningfulness of the considered analysis. Focusing on the buildings information (in terms of positioning, volume, floors, shape), we have exploited the data available from OpenStreetMap, a freely available database allowing exportation of the saved data (see e.g., [1]). In particular, the raw information retrieved from OpenStreetMap has been processed by QGIS software, in order to filter the subset of buildings falling within each area of interest (i.e., Spinaceto or Ponte-Parione).

Focusing on the sensitive buildings, we have selected schools and medical buildings based on online information publicly available from the municipality. In the following step, we have used QGIS to filter the set of sensitive buildings (as a ShapeFile) from the entire set of buildings in each scenario.

Focusing then on population data, we have exploited the 2011 census done by ISTAT - the Italian national statistics institute - and freely available from [2], in order to obtain the number of children/teenagers and adults in each building of the scenario. Although such information is not apparently up-to-date (as more than 10 years passed from the last census), we believe that it is in any case reliable and able to capture the current population conditions for the areas under investigation, due to the following reasons: *i*) national population has not substantially increased in the last 10 years, *ii*) both Spinaceto and Ponte-Parione have been pervasively inhabited much earlier than 10 years ago, *iii*) the urbanization level (in terms of buildings and their exploitation) has not substantially changed over the last 10 years in the considered neighborhoods.



(a) Spinaceto



(b) Ponte-Parione

Fig. 8. Breakdown of the population age. The population bins belonging to children and teenagers category are highlighted.

Fig. 8 reports the number of inhabitants retrieved from the national census over the two scenarios, for different age bins. Two considerations hold by analyzing the figure. First, the distribution of inhabitants over the bins is rather similar over the two scenarios. Second, the number of inhabitants belonging to children and teenagers bins is not marginal, i.e., always more than 1500 for Spinaceto and more than 700 in Ponte-Parione for each bin.

However, we point out that the population data collected by ISTAT is referred to census zones, i.e., small portions of territory - each of them composed of multiple buildings. On the contrary, our approach requires as input the population information for each building. To solve this issue, we have initially loaded the census zones on QGIS software. In the following step, we have assigned each building b of the scenario to its corresponding census zone z .

TABLE I
BUILDINGS AND POPULATION COMPARISON OVER THE
CONSIDERED SCENARIOS.

Metric Name	Metric Value	
	Spinaceto	Ponte-Parione
Size of the area	3.51 km ²	1.62 km ²
Number of buildings	1068	755
Building density	304/km ²	466/km ²
Number of schools	16	6
Number of school buildings	58	14
Number of medical centers	4	4
Number of medical buildings	30	34
Number of inhabitants	29987	19265
Inhabitants density	8543/km ²	11892/km ²
Number of children and teenagers	6298	3278
Children and teenagers density	1974/km ²	2023/km ²

Finally, we have computed the number of children/teenagers $N_b^{\text{CHD-TN}}$ and the number of adults N_b^{AD} in each building as:

$$N_b^{\text{CHD-TN}} = \frac{N_z^{\text{CHD-TN}} \cdot V_b}{V_z} \quad (1)$$

$$N_b^{\text{AD}} = \frac{N_z^{\text{AD}} \cdot V_b}{V_z} \quad (2)$$

where $N_z^{\text{CHD-TN}}$ (N_z^{AD}) is the number of children/teenagers (adults) of census zone z , V_b is the volume of building b , and V_z is the volume of all buildings falling within census zone z . The output of this step is then a building map (as a ShapeFile), enriched with the population information.

Finally, Tab. I summarizes the main building and population information collected in the two scenarios. More in depth, the area in Spinaceto is larger than Ponte-Parione, being also characterized by an higher number of buildings. However, the building density in Spinaceto is lower than the one in Ponte-Parione. Focusing then on the sensitive buildings, Spinaceto hosts a larger number of schools compared to Ponte-Parione. However, the number of medical centers is comparable over the two scenarios. Clearly, each school and medical center is composed of multiple buildings. Eventually, the number of children/teenagers and inhabitants is higher in Spinaceto compared to Ponte-Parione. However, the opposite holds when considering the population density. Finally, the total number of children and teenagers is rather large, i.e., several thousands in each scenario.

B. Tower Data

The second step required as input to our analysis is the collection of data to characterize the towers

TABLE II
TOWER CHARACTERIZATION.

Feature ID	Feature	Description
F1	Type	Roof-top or raw-land
F2	Positioning	GPS coordinates and altitude
F3	Operators	Number and IDs
F4	Sectors	Number of sectors, sector orientation (per operator)
F5	Radiating sources	Number of panels, panel setup (per sector)

in the considered scenarios. As reported in Tab. II, the tower characterization includes the following features: *F1*) tower type (roof-top or raw-land), *F2*) tower positioning, *F3*) operators hosted in each tower, *F4*) number of sectors for each operator and orientation of each sector, *F5*) radio configuration for each sector (in terms e.g., of installed panels and radio configuration of each panel).

Given the aforementioned huge and detailed amount of information, two natural questions emerge: How to collect such information over the territory? Is such information able to capture the evolution of the network in the coming years? To tackle both questions in a comprehensive and meaningful way, in this work we have adopted a hybrid approach, in which *F1*)-*F4*) are sensed from the real deployments realized in the considered scenarios, while *F5*) is derived from reasonable assumptions about pre-5G and 5G deployments and realistic radio configurations for each installed antenna panel. However, the skeptic of our work may object that we are not directly sensing *F5*) from the actual deployment over the territory, and hence our results are not meaningful. Before going into the details of the collected input data, let us first analyze such concern and better motivate the meaningfulness of our hybrid approach.

1) *Hybrid Approach: Motivation:* Since we are currently in the early days of 5G deployment, not all the towers in the scenario host 5G equipment - many of them provide only pre-5G connectivity. However, it is expected that 5G technology will become predominant in the next (few) years, meaning that the panels installed on the towers will be progressively updated/replaced to dismiss legacy equipment (e.g., 3G antennas [3]) in favor of 5G radiating elements. This picture is further complicated in the Italian country, as the presently enforced exposure limits are more stringent than the ones proposed by international organizations (such as ICNIRP [4])

and promoted by the European Commission. According to previous works (see e.g., [5], [6]), strict exposure regulations negatively impact co-location of antennas on the same tower (and even installation of new towers on the same building), thus (possibly) introducing strong barriers on the deployment of 5G networks. In countries adopting stricter-than-ICNIRP regulations, in fact, urban sites tend to be almost saturated in terms of available EMF space - and therefore it is not possible to install new radiating sources (without violating the exposure limits). As a result, more towers have to be installed over the territory compared to countries adopting ICNIRP regulations [5]. This picture has changed in some European countries, like Poland and Lithuania, which have updated their national regulations from stricter-than-ICNIRP to ICNIRP-based regulations.

In this context, the application of ICNIRP or stricter-than-ICNIRP regulations influences the input data required by our work, as intuitively, the set of radiating elements, and their radiated power, strongly depends on the adopted regulation. In this work, we have chosen to derive a deployment that satisfies the limits for general public defined by ICNIRP [4], due to the following reasons. First, we are able to generalize our results to the (many) countries adopting the ICNIRP regulations. Second, we consider a conservative setting, in which the exposure is (likely) higher than the one currently experienced over the territory - resulting from stricter-than-ICNIRP regulations.

Obviously, an exposure regulation has an impact also on the planning on the network, in terms e.g., of tower positioning, sector orientation, radiated power setting, etc. In our case, we solve this issue by adopting a hybrid approach, in which we retrieve the actual tower positioning and sector orientation, while we define configurations of the radiating sources that satisfy ICNIRP regulations. We believe that this approach is representative of a worst-case scenario (in terms of exposure), due to the following reasons: *i*) higher tower density resulting from the stricter-than-ICNIRP planning compared to the ICNIRP one [5], *ii*) radiated power from each source satisfying ICNIRP limits (thus higher than the stricter-than-ICNIRP case).

2) *Collection of tower information:* We then provide more details about how the information $F1)$ - $F4)$ has been sensed from Spinaceto and Ponte-Parione. More in depth, we initially extract the re-

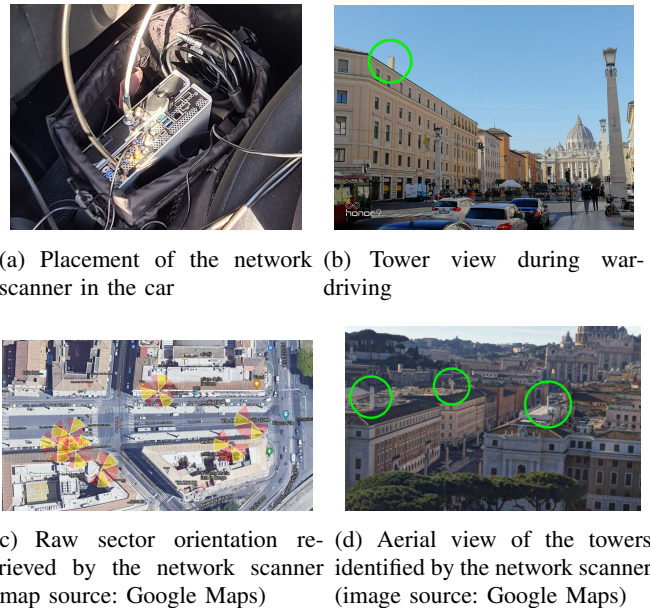


Fig. 9. War-driving step performed with the network scanner.

levant data from the documents sent by operators to ARPA Lazio in order to get authorization approval for the tower.² The collected information includes tower type (roof-top vs. raw-land), GPS positioning of the tower, installed operators, number of sectors and sectors orientation for each tower. In the following step, we perform a cross-check of the obtained data through a war-driving based approach. A tower check over the territory is in fact mandatory, due to the following reasons: *i*) the information reported in the tower authorization documents may be outdated (as subsequent tower updates performed after the initial authorization may not generate new authorization requests - this include e.g., tower disposal), *ii*) authorization documents are not available for all the towers (e.g., some towers in Ponte-Parione are placed on buildings belonging to the Vatican state - and those authorization requests are not processed by ARPA Lazio).

More concretely, the tower check is done in the following way. We install a Rohde&Schwarz TSMA6 network scanner on a car, as shown Fig. 9(a). The network scanner is then connected to a PCTEL P286H external omnidirectional antenna (mounted on the roof on the car). In addition, electricity to the network scanner is provided through a plug on the car. The scanner is then complemented by a tablet, wirelessly connected to the scanner, and

²No sensitive information reported in the authorization documents is disclosed in our work.

TABLE III
RADIO CONFIGURATION FOR A SINGLE SECTOR s_1 OF ROOF-TOP TYPE.

Antenna ID a	1	2	3	4	5	6	7	8
Frequency Band F_a	700 MHz	800 MHz	900 MHz	1800 MHz	2100 MHz	2600 MHz	3700 MHz	26000 MHz
Technology	5G	4G	2G	4G	4G	4G	5G	5G
Antenna Panel p	QuadriBand						5G-midBand	5G-mmWave
Mechanical Tilt $\sigma_{(s_1,p)}$	0°							
Electrical Tilt t	2°	4°	2°	4°			2°	0°
Output Power $P_{(s_1,a)}^{\text{MAX}}$	40 W			60 W			80 W	5 W
Maximum Gain $G_{(s_2,a)}^{\text{MAX}}$	13.8 dBi	14.4 dBi	14.9 dBi	16.4 dBi	17.5 dBi	17.7 dBi	23.9 dBi	33.5 dBi
Horiz. Diagram $D_{(s_1,a)}^{\text{H}}$	MSI file (F_{a_1}, t_1)	MSI file (F_{a_2}, t_2)	MSI file (F_{a_3}, t_3)	MSI file (F_{a_4}, t_4)	MSI file (F_{a_5}, t_5)	MSI file (F_{a_6}, t_6)	MSI file (F_{a_7}, t_7)	MSI file (F_{a_8}, t_8)
Vert. Diagram $D_{(s_1,a)}^{\text{V}}$	MSI file (F_{a_1}, t_1)	MSI file (F_{a_2}, t_2)	MSI file (F_{a_3}, t_3)	MSI file (F_{a_4}, t_4)	MSI file (F_{a_5}, t_5)	MSI file (F_{a_6}, t_6)	MSI file (F_{a_7}, t_7)	MSI file (F_{a_8}, t_8)
Reduction Factor R_p	1						α_p^{5G}	

TABLE IV
RADIO CONFIGURATION FOR A SINGLE SECTOR s_2 OF RAW-LAND TYPE.

Antenna ID a	1	2	3	4	5	6	7	8
Frequency Band F_a	700 MHz	800 MHz	900 MHz	1800 MHz	2100 MHz	2600 MHz	3700 MHz	26000 MHz
Technology	5G	4G	2G	4G	4G	4G	5G	5G
Antenna Panel p	QuadriBand						5G-midBand	5G-mmWave
Mechanical Tilt $\sigma_{(s_2,p)}$	0°							
Electrical Tilt	4°	6°	4°	6°			2°	0°
Output Power $P_{(s_2,a)}^{\text{MAX}}$	60 W			80 W			100 W	5 W
Maximum Gain $G_{(s_2,a)}^{\text{MAX}}$	13.8 dBi	14.4 dBi	14.9 dBi	16.4 dBi	17.5 dBi	17.7 dBi	23.9 dBi	33.5 dBi
Horiz. Diagram $D_{(s_2,a)}^{\text{H}}$	MSI file (F_{a_1}, t_1)	MSI file (F_{a_2}, t_2)	MSI file (F_{a_3}, t_3)	MSI file (F_{a_4}, t_4)	MSI file (F_{a_5}, t_5)	MSI file (F_{a_6}, t_6)	MSI file (F_{a_7}, t_7)	MSI file (F_{a_8}, t_8)
Vert. Diagram $D_{(s_2,a)}^{\text{V}}$	MSI file (F_{a_1}, t_1)	MSI file (F_{a_2}, t_2)	MSI file (F_{a_3}, t_3)	MSI file (F_{a_4}, t_4)	MSI file (F_{a_5}, t_5)	MSI file (F_{a_6}, t_6)	MSI file (F_{a_7}, t_7)	MSI file (F_{a_8}, t_8)
Reduction Factor R_p	1						α_p^{5G}	

TABLE V
STATISTICAL REDUCTION FACTORS FOR THE DIFFERENT LEVELS OF 5G ADOPTION.

5G Adoption Level		α_p^{5G} values	
Name	Index l	Ponte-Parione	Spinaceto
Early	1	0.03	0.05
Medium	2	0.13	0.21
Maturity	3	0.18	0.31

running the Rohde&Schwarz ROMES4 commercial software for data acquisition and analysis. We then extensively cover the streets in the considered scenarios, focusing in particular on the zones where we identified the towers (Fig. 9(b)). Based on the triangularization of the acquired signals, the software is able to position the identified towers on a map, showing also the sector orientation (Fig. 9(c)). This last information is instrumental for towers without available authorization data, particularly those ones for which sector orientation is hidden to sight (like the fake chimney in Fig. 9(b)). Clearly, the raw information presented by the software (Fig. 9(c)) has to be manually filtered, in order to remove duplicates and/or not precise tower positioning.

Eventually, Fig. 9(d) reports the towers that were completely characterized through the war-driving approach (i.e., those ones with missing authorization data). For all the other towers (i.e., the ones with available authorization), the war-driving approach allowed identifying the active ones and discarding the disposed ones. In addition, sector information was compared against the one reported in the authorization documents, finding in general a good matching between both sources.

3) *Radio Configuration*: The last phase of the tower characterization is the configuration of the radiating sources for each sector. This step includes the setting of several parameters, ranging from the selection of the adopted panels to the configuration of the radio features for each panel. Without loss of generality, in this work we adopt an uniform radio configuration for all the sectors and all the operators, as shown in Tab. III and Tab. IV for the roof-top and raw-land cases. More in depth, we adopt real parameters and realistic settings, by assuming the deployment of three distinct antenna panels for each sector (and each operator), namely: a quadri-band

TABLE VI
EXAMPLE OF A TOWER HOSTING TWO OPERATORS AND THREE SECTORS PER OPERATOR.

Operator	Number of sectors	Sectors Orientation ρ_s^{CLOCK}	Electrical center height of panel p (above sea level)		
			Quadriband	5G-MidBand	5G-mmWave
A	3	$\{80^\circ, 200^\circ, 280^\circ\}$	78.3 m	78.8 m	77.4 m
B	3	$\{70^\circ, 220^\circ, 330^\circ\}$	76 m	76.5 m	75.1 m

TABLE VII
TOWER METRICS OVER THE CONSIDERED SCENARIOS.

Metric Name	Metric Value	
	Ponte-Parione	Spinaceto
Number of operators	4	
Number of towers	45	13
Number of roof-top towers	45	10
Number of raw-land towers	0	3
Number of pre-5G sources	934	354
Number of 5G sources	560	212

antenna panel, a mid-band panel and mm-Wave one. The positioning (in scale) of the aforementioned panels in roof-top and raw-land cases is shown in Fig. 3.

Clearly, the main application for mm-Wave panels is to boost capacity (especially in small cell deployments). However, we believe that including a mm-Wave panel on a tower is meaningful in our scenario, due to the following reasons: *i*) authorization requests to install mm-Wave antennas over towers have been already received (thus demonstrating that the operators are keen to invest on towers for the installation of mm-Wave panels), *ii*) towers are normally located close to densely populated areas, including main streets - where 5G over mm-Wave may be instrumental to provide high-level and innovative services.

We then provide more details about the parameters reported in Tab. III-Tab. IV. Naturally, the quadri-band panel includes sub-GHz band of 5G, as well as the bands for 2G and 4G. In addition, the values for the mechanical/electrical tilting and the output power are taken from typical settings adopted by operators. Eventually, the output power of the mm-Wave panel is set to the maximum one allowed by the equipment under consideration. The antenna gains reported in the tables are retrieved from the datasheets of the panels. Moreover, the radiation diagrams for each source are taken from the real ones made available by the antenna vendors. Such information is included in files with MSI format (i.e., a list of gain values for each angle in horizontal and vertical planes). Each radiation

diagram depends on the following features: *i*) the panel model (highlighted with different colors in the tables), *ii*) the operating frequency, and *iii*) the electrical tilting value. Finally, the last row of Tab. III-IV reports the reduction factor that is applied to the maximum power. In this work, we assume that the quadri-band panel always radiates at the maximum power (corresponding to the values of output power reported in the tables). On the other hand, the output power of mid-band and mm-Wave panels p is scaled by the factor α_p^{5G} , which is set in accordance to the realistic values provided by relevant standards [7].

More in depth, α_p^{5G} captures the statistical reduction factors that are introduced by the smart antenna management features of 5G over mid-band and mm-Wave. More concretely, Tab. V reports the reduction factors over the two scenarios and the different level of 5G adoptions. The numerical values are taken from [7], by assuming that Spinaceto is representative for a sparse area while Ponte-Parione for a dense one. In addition, the early/medium/maturity levels of 5G adoption correspond to 5%/50%/95% utilization level of [7], respectively. By observing the values in Tab. V, two considerations emerge. First, strong reduction factors are applied even in the maturity case. Second, the reduction factors are lower (i.e., stronger) in Spinaceto than in Ponte-Parione, due to the lower and less uniform building density that characterizes the former with respect to the latter.

For the sake of clarity, Tab. VI reports the sector information for a roof-top tower in Spinaceto. In this case, the tower hosts two operators, each of them managing three sectors. For each sector, the radio configuration in Tab. III is implemented. Tab. VI details also the altitude of the electrical center for each panel type. The altitude of the each panel is retrieved in this way: *i*) the roof-altitude is retrieved from OpenStreetMap database, *ii*) based on the number of operators and number of sectors, a roof-top installation is defined (based on e.g., Fig. 3), *iii*) the altitude in *i*) is summed to the height of the each

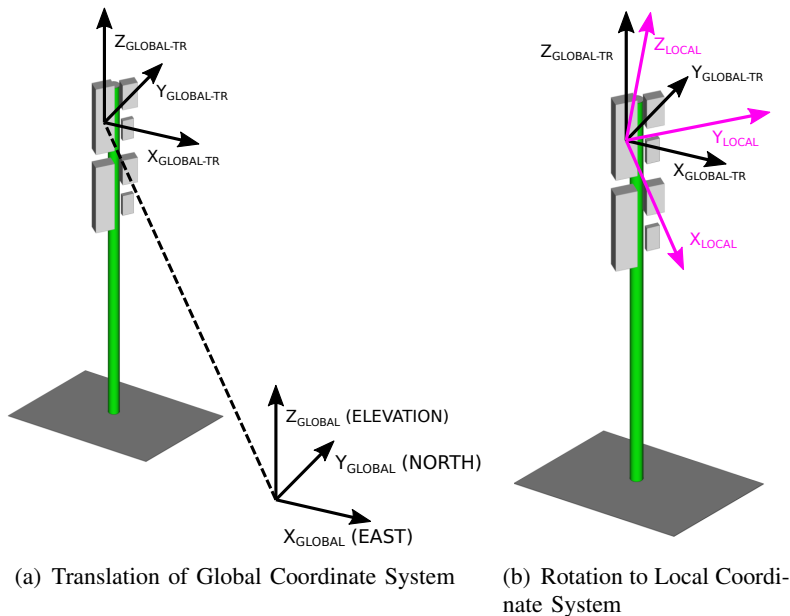


Fig. 10. Change from global coordinate system to the local coordinate system of a given panel p .

panel in the installation.

Eventually, Tab. VII reports some relevant tower metrics over Spinaceto and Ponte-Parione. More in depth, all four national operators manage towers in both scenarios. However, the number of towers in Ponte-Parione is larger than in Spinaceto. Focusing on the tower type, Ponte-Parione includes only rooftop installations, while Spinaceto hosts also some raw-lands. Obviously, the total number of both pre-5G and 5G sources is clearly higher in Ponte-Parione than in Spinaceto. However, we point out that the number of pre-5G sources is always higher than the 5G ones, due to the larger number of frequency bands managed by the formers (800, 900, 1800, 2100, 2600 MHz) with respect to the latter (700, 3600, 26000 MHz).

C. Exposure Assessment Procedure

In this part, we provide more details about the procedure to perform the exposure assessment, given as input the tower and building information. We initially focus on the exposure assessment for a generic pixel c over the territory, by considering the EMF that is radiated over c by antenna a of panel p installed at sector s . The considered methodology is fully compliant with the national exposure assessment procedure currently adopted in Italy [8]–[10], which is in turn based on relevant international exposure assessment standards [11].

More in depth, the sector orientation ρ_s^{CLOCK} is normally provided in counter-wise degrees, starting from the North axis. In our assessment, however, the sector orientation ρ_s is defined in counter-wise degrees from East axis. Consequently, ρ_s is expressed as:

$$\rho_s = \begin{cases} \frac{\pi}{2} - \rho_s^{\text{CLOCK}} & \text{if } 0 \leq \rho_s^{\text{CLOCK}} \leq \pi/2 \\ \frac{5}{2}\pi - \rho_s^{\text{CLOCK}} & \text{if } \pi/2 < \rho_s^{\text{CLOCK}} \leq 2\pi \end{cases} \quad (3)$$

The following step is the change of the global coordinate system to the local one of the considered panel. This step is fundamental in order to properly compute the relative orientation of the pixel with respect to the antenna panel, and consequently for a thorough assessment of exposure. Fig. 10 sketches the steps that have to be applied in order to adopt the local coordinate system of the panel. More concretely, a translation is applied first (Fig. 10(a)), in order to move the coordinate system center on the electrical center of the panel. In the following step, a rotation is performed (Fig. 10(b)), in order to align the coordinate system to the relative orientation in space of the panel.

More formally, let us denote with $[x_{(s,p)}, y_{(s,p)}, z_{(s,p)}]$ the 3D global coordinates of the antenna panel p of sector s . In a similar way, let us denote with $[x_c, y_c, z_c]$ the global coordinates of pixel c . Our goal is then to apply the change of coordinate system shown in Fig. 10 in order to obtain the local coordinates $[\tilde{x}_{(c,s,p)}, \tilde{y}_{(c,s,p)}, \tilde{z}_{(c,s,p)}]$

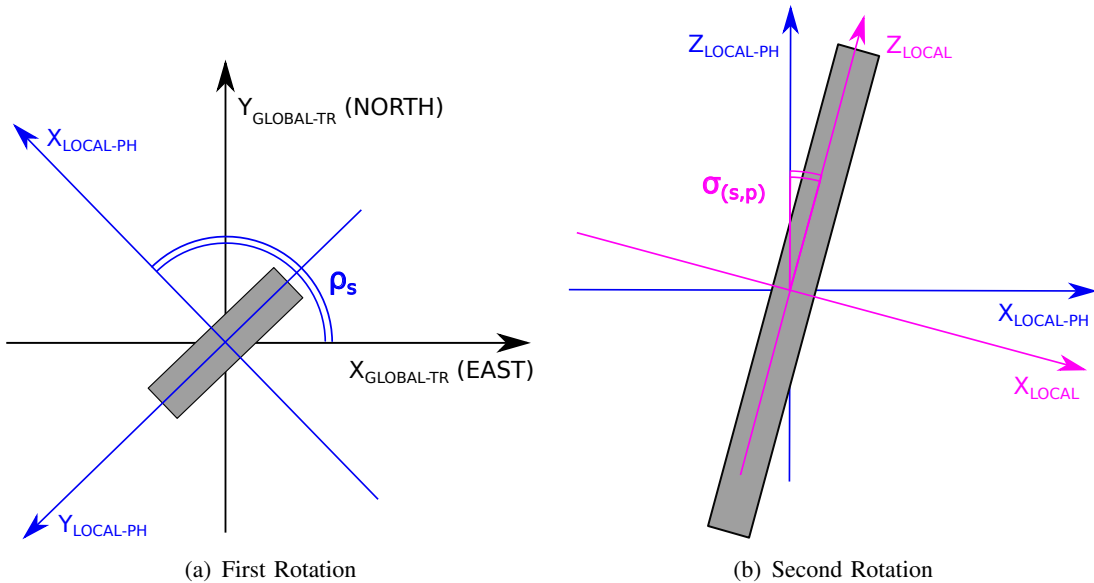


Fig. 11. Graphical sketch of the rotations applied in $\Gamma_{(s,p)}$

of c with respect to panel p in s . To this aim, we apply first the translation to the local system and then the rotation with the following equation:

$$\underbrace{\begin{bmatrix} \tilde{x}_{(c,s,p)} \\ \tilde{y}_{(c,s,p)} \\ \tilde{z}_{(c,s,p)} \end{bmatrix}}_{\text{Local coordinates}} = \underbrace{\Gamma_{(s,p)}}_{\text{Rotation}} \cdot \underbrace{\begin{bmatrix} x_c - x_{(s,p)} \\ y_c - y_{(s,p)} \\ z_c - z_{(s,p)} \end{bmatrix}}_{\text{Translation}} \quad (4)$$

where $\Gamma_{(s,p)}$ is the rotation matrix, formally expressed as:

$$\Gamma_{(s,p)} = \begin{bmatrix} \cos \rho_s \cos \sigma_{(s,p)} & \sin \rho_s \cos \sigma_{(s,p)} & -\sin \sigma_{(s,p)} \\ -\sin \rho_s & \cos \rho_s & 0 \\ \cos \rho_s \sin \sigma_{(s,p)} & \sin \rho_s \sin \sigma_{(s,p)} & \cos \sigma_{(s,p)} \end{bmatrix} \quad (5)$$

where we recall that ρ_s is the orientation of sector s , while $\sigma_{(s,p)}$ is the mechanical tilting of panel p from sector s . A graphical sketch of the rotations in $\Gamma_{(s,p)}$ is shown in Fig. 11. Intuitively, the first rotation aligns the x axis of the local system to the sector orientation, while the second one matches the z axis with the actual mechanical tilting of the panel.

In the following step, the 3D distance of the pixel c with respect to the panel p in s is computed:

$$r_{(c,s,p)} = \sqrt{(x_c - x_{(s,p)})^2 + (y_c - y_{(s,p)})^2 + (z_c - z_{(s,p)})^2} \quad (6)$$

We then concentrate on the assessment of the orientation of c with respect to p in s . To this aim, we introduce horizontal plane and vertical plane angles, formally expressed as $\theta_{(c,s,p)}$ and $\phi_{(c,s,p)}$. A graphical sketch, useful to understand how such

angles are derived, is shown in Fig. 12. $\theta_{(c,s,p)}$ and $\phi_{(c,s,p)}$ are then formally expressed as:

$$\theta_{(c,s,p)} = \text{asin} \left(\frac{\tilde{z}_{(c,s,p)}}{r_{(c,s,p)}} \right) \quad (7)$$

$$\phi_{(c,s,p)} = \text{asin} \left(\frac{\tilde{y}_{(c,s,p)}}{\sqrt{r_{(c,s,p)}^2 - \tilde{z}_{(c,s,p)}^2}} \right) \text{sgn}(\tilde{x}_{(c,s,p)}) + \frac{\pi}{2} \text{sgn}(\tilde{y}_{(c,s,p)})(1 - \text{sgn}(\tilde{x}_{(c,s,p)})) \quad (8)$$

At this point, we are able to compute the gain $G_{(c,s,a)}$ from antenna a of panel p installed over sector s that is received over c , which is expressed as in [8], [9]:

$$G_{(c,s,a)} = G_{(s,a)}^{\text{MAX}} \cdot D_{(s,a)}^{\text{V}}(\theta_{(c,s,p)}) \cdot D_{(s,a)}^{\text{H}}(\phi_{(c,s,p)}) \quad (9)$$

where $G_{(s,a)}^{\text{MAX}}$ is the gain of antenna element a of sector s and $D_{(s,a)}^{\text{V}}$ and $D_{(s,a)}^{\text{H}}$ are the numerical gain values on the horizontal and vertical planes (respectively). In our scenarios, we assume that $D_{(s,a)}^{\text{V}}$ and $D_{(s,a)}^{\text{H}}$ are provided in a linear scale in terms of scaling terms (lower than unity). We recall that $D_{(s,a)}^{\text{V}}$ and $D_{(s,a)}^{\text{H}}$ are extracted from the MSI files of each antenna a (which in turn depend also on the adopted frequency and the electrical tilting as shown in Tab. III-IV).

We then apply the model of [8]–[10] (which is almost equivalent to the point-source model of ITU [12]), to evaluate the EMF over pixel c , radiated by

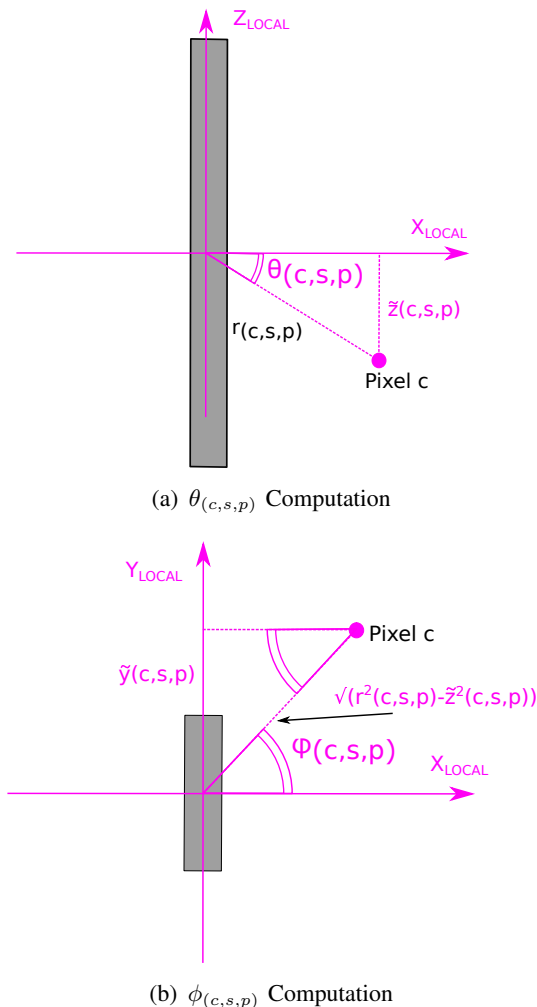


Fig. 12. Graphical sketch for the computations of $\theta_{(c,s,p)}$ and $\phi_{(c,s,p)}$.

antenna a from sector s . More formally, the exposure in terms of power density $S_{(c,s,a)}$ is expressed as:

$$S_{(c,s,a)} = \frac{P_{(s,a)}^{\text{MAX}} \cdot G_{(c,s,a)} \cdot R_p}{4\pi \cdot r_{(c,s,a)}^2 \cdot A_{(c,s,a)}} \quad (10)$$

where $P_{(s,a)}^{\text{MAX}}$ is the maximum output power, R_p is the power reduction factor, $A_{(c,s,a)}$ is the attenuation over pixel c .

The total power density S_c^{TOT} from all antennas is then expressed as:

$$S_c^{\text{TOT}} = \sum_s \sum_a S_{(c,s,a)} \quad (11)$$

The total power density from 5G antennas is denoted as:

$$S_c^{5G} = \sum_s \sum_a S_{(c,s,a)}, \forall a : F_a \in \mathcal{F}^{5G} \quad (12)$$

where $\mathcal{F}^{5G} = \{700, 3700, 26000 \text{ MHz}\}$.

Similarly, the total power density from pre-5G antennas is expressed as:

$$S_c^{\text{PRE-5G}} = \sum_s \sum_a S_{(c,s,a)}, \forall a : F_a \in \mathcal{F}^{\text{PRE-5G}} \quad (13)$$

where $\mathcal{F}^{\text{PRE-5G}} = \{800, 900, 1800, 2100, 2600 \text{ MHz}\}$.

Finally, the electric field $E_c^{(\cdot)}$ of each of the previous terms is computed out from the power density $S_c^{(\cdot)}$ by assuming far-field conditions:

$$E_c^{(\cdot)} = \sqrt{S_c^{(\cdot)} \cdot 377} \quad (14)$$

Up to this point, we have shed light on the exposure evaluation for a generic pixel c . Let us then provide more details on the computation of the exposure for each building b . To this aim, we generate a grid of pixels in the horizontal plane with a tight resolution (i.e., $2 \times 2 \text{ m}$). We then exploit QGIS to filter the subset of pixels in each building. In addition, each pixel is enriched with the roof altitude of the building taken from the map of the scenario. In the following step, we apply Eq. (3)-(14) to compute the electric field for each pixel c . Finally, we compute the average building exposure $E_b^{(\cdot)}$ as the root mean square exposure from all the pixels belonging to b .

D. Generation of the figures

In this part, we provide more details about the generation of Fig. 4-7.

Average EMF over the buildings - Fig. 4. Step 1: computation of E_c^{TOT} for each adoption level (based on 5G reduction factors of Tab. V); Step 2: computation of building exposure E_b^{TOT} ; Step 3: computation of the average exposure over: all buildings, schools, medical centers.

Average EMF over children and teenagers - Fig. 5. Step 1: computation of E_c^{TOT} , $E_c^{\text{PRE-5G}}$, E_c^{5G} for each adoption level (based on 5G reduction factors of Tab. V); Step 2: computation of building exposure E_b^{TOT} , $E_b^{\text{PRE-5G}}$, E_b^{5G} ; Step 3: computation of the average exposure over children and teenagers from the building exposure in Step 2, weighed by the number of children and teenagers in the building $N_b^{\text{CHD-TN}}$.

Percentage of children/teenagers, school buildings and medical buildings vs. EMF exposure - Fig. 6. Step 1: computation of E_c^{TOT} , $E_c^{\text{PRE-5G}}$,

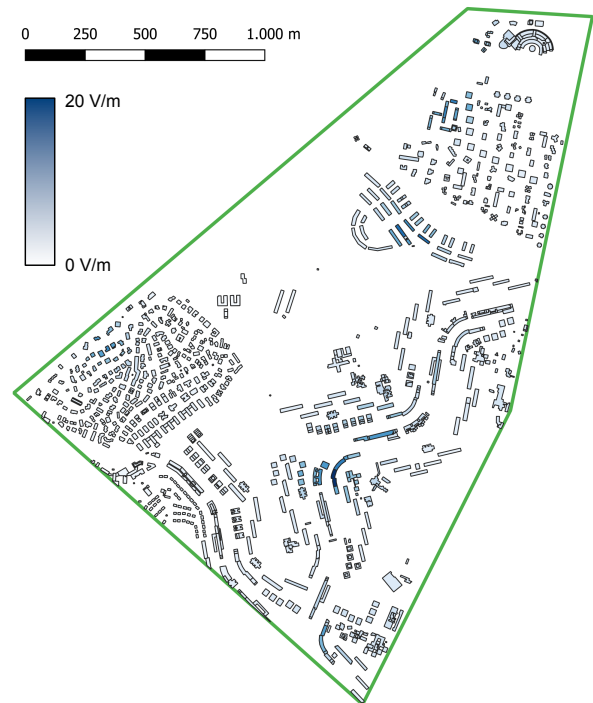
E_c^{5G} for each adoption level (based on 5G reduction factors of Tab. V); Step 2: computation of building exposure E_b^{TOT} , E_b^{PRE-5G} , E_b^{5G} ; Step 3: computation of the exposure over children and teenagers from the building exposure in Step 2, weighed by the number of children and teenagers in the building N_b^{CHD-TN} ; Step 4: computation of the Empirical Cumulative Distribution Function (ECDF) for each category (children/teenagers, school buildings, medical buildings), each type of source (pre-5G, 5G) and each level of 5G adoption (early, medium, maturity).

Impact of introducing the building attenuation
- **Fig. 7.** Step 1: computation of E_c^{TOT} , E_c^{PRE-5G} , E_c^{5G} for each adoption level (based on 5G reduction factors of Tab. V) and each level of attenuation; Step 2: computation of building exposure E_b^{TOT} , E_b^{PRE-5G} , E_b^{5G} ; Step 3: computation of the average exposure over children and teenagers from the building exposure in Step 2, weighed by the number of children and teenagers in the building N_b^{CHD-TN} .

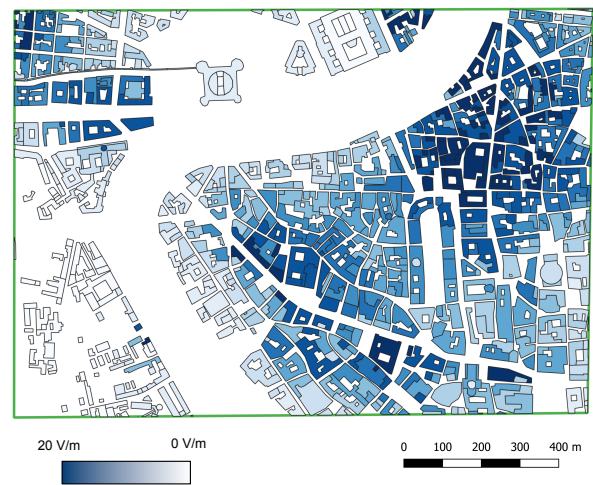
E. Additional Results

In the last part of this Appendix, we provide a set of additional outcomes, useful to complement Fig. 4-7. More in depth, Fig. 13 visually highlights the total exposure over buildings in Spinaceto and Ponte-Parione, by imposing a maturity level for 5G. Interestingly, the exposure over buildings strongly varies across the two scenarios. Spinaceto is characterized by a relatively low amount of exposure, being the highest value (colored in dark blue color) limited to the few buildings close to the tower installations. On the other hand, the relatively higher tower density in Ponte-Parione compared to Spinaceto also results in higher exposure buildings (as expected). Clearly, the zones in Ponte-Parione that are characterized by a low tower density (like the one show in bottom-left part of Fig. 13(b)) are also the ones in which the buildings receive a small amount of exposure.

Fig. 14 details the exposure levels that are received by the following categories: *i*) children/teenagers vs. adults vs. entire population (Fig. 14(a)-14(c)), *ii*) schools vs. medical buildings vs. all buildings (Fig. 14(b)-14(d)). Three considerations hold by analyzing Fig. 14. First, all the categories of people receive similar exposure levels. This outcome derives from the distributions of children/teenagers and adults over the territory, which are



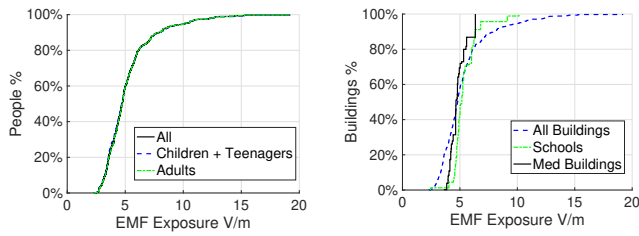
(a) Spinaceto



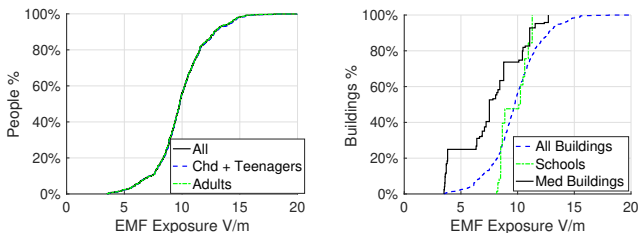
(b) Ponte-Parione

Fig. 13. EMF exposure over the buildings (5G maturity setting).

rather similar in the scenarios under considerations. Second, schools and medical buildings tend to receive different exposure levels compared to the category including all the buildings. Naturally, this is due to the fact that schools and medical buildings represent a small fraction of the total buildings, and therefore the positioning of each sensitive building, as well as the relative positioning of the towers in its surroundings, play a key role in determining the actual exposure levels. Third, the composite exposure is overall lower than the ICNIRP limits for the

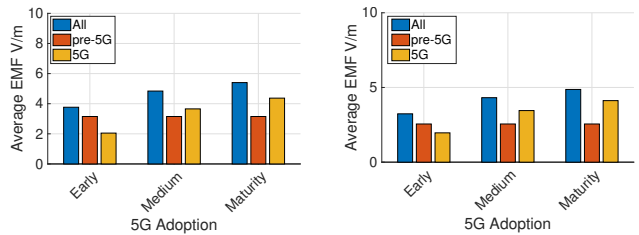


(a) Percentage of people vs. EMF exposure - Spinaceto. (b) Percentage of buildings vs. EMF exposure - Spinaceto.

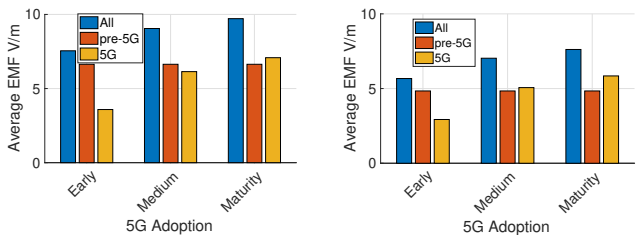


(c) Percentage of people vs. EMF exposure - Ponte-Parione. (d) Percentage of buildings vs. EMF exposure - Ponte-Parione.

Fig. 14. Exposure levels for children/teenagers against adults and entire population (left). Comparison of exposure levels vs. the type of the building (right). Figures retrieved with a 5G maturity level.



(a) Schools - Spinaceto (b) Med. Buildings - Spinaceto



(c) Schools - Ponte-Parione (d) Med. Buildings - Ponte-Parione

Fig. 15. Impact of the 5G adoption level on the average exposure over schools (left) and med. buildings (right).

general public over the considered frequency range (between 36 V/m and 61 V/m), thus guaranteeing adherence to international exposure guidelines.

Finally, Fig. 15 reports the average EMF over schools and medical buildings, by differentiating between: *i*) type of exposure sources (all, only 5G, only pre-5G), 5G adoption level (early, medium, maturity) and considered scenario (Spinaceto and Ponte-Parione). Overall, the exposure is proportional to the adoption level (as expected). In ad-

dition, the exposure in Ponte-Parione is higher than the one in Spinaceto (thus confirming the outcomes of Fig. 5). Finally, the contribution of 5G exposure is higher than the pre-5G when considering a 5G maturity level (again in line with Fig. 5).

REFERENCES

- [1] *OpenStreetMap Data Extracts*. Available at <http://download.gofabrik.de/>, last accessed on 14th Dec. 2021.
- [2] *Basi Territoriali e Variabili Censuarie*. Available at <https://www.istat.it/it/archivio/104317>, last accessed on 14th Dec. 2021.
- [3] *TIM closes the 3G network! Those who own a SIM of less than 128k will have to replace it: here's how*. Available at <https://www.italy24news.com/News/248423.html>, Last Accessed: 17th Jan. 2022.
- [4] International Commission on Non-Ionizing Radiation Protection (ICNIRP), "ICNIRP guidelines on limiting exposure to time-varying electric, magnetic and electromagnetic fields (100 kHz to 300 GHz)." Available at: <https://www.icnirp.org/cms/upload/publications/ICNIRPrfgrdl2020.pdf>, Jul. 2020. Last Accessed: 29th Sept. 2020.
- [5] *ITU-T K.Sup14 : The impact of RF-EMF exposure limits stricter than the ICNIRP or IEEE guidelines on 4G and 5G mobile network deployment*. Available at <https://www.itu.int/rec/T-REC-C-K.Sup14-201805-I>, last accessed on 25th July 2018.
- [6] L. Chiaraviglio, A. S. Cacciapuoti, G. Di Martino, M. Fiore, M. Montesano, D. Trucchi, and N. B. Melazzi, "Planning 5G networks under EMF constraints: State of the art and vision," *IEEE Access*, vol. 6, pp. 51021–51037, 2018.
- [7] *IEC TR 62669 – Edition 2.0 2019/04 - Case Studies supporting IEC 62232 – Determination of RF field strength, power density and SAR in the vicinity of radiocommunications base stations for the purpose of evaluating human exposure*. Available at <https://webstore.iec.ch/publication/62014>, last accessed on 12th Jan. 2022.
- [8] *Guida alla realizzazione di una Stazione Radio Base per rispettare i limiti di esposizione ai campi elettromagnetici in alta frequenza - v0*. Available at <https://mycatalogo.ceinorme.it/cei/item/000006456?lang=en>, last accessed on 12th Jan. 2022.
- [9] *Guida alla realizzazione di una Stazione Radio Base per rispettare i limiti di esposizione ai campi elettromagnetici in alta frequenza - v1*. Available at <https://mycatalogo.ceinorme.it/cei/item/001007184?lang=en>, last accessed on 12th Jan. 2022.
- [10] *Guida alla realizzazione di una Stazione Radio Base per rispettare i limiti di esposizione ai campi elettromagnetici in alta frequenza - v2*. Available at <https://mycatalogo.ceinorme.it/cei/item/0010017895?sso=y&lang=en>, last accessed on 12th Jan. 2022.
- [11] *IEC 62232:2017 Determination of RF field strength, power density and SAR in the vicinity of radiocommunication base stations for the purpose of evaluating human exposure*. Available at <https://webstore.iec.ch/publication/28673>, last accessed on 25th Sept. 2020.
- [12] *ITU-T K.70 Mitigation techniques to limit human exposure to EMFs in the vicinity of radiocommunication stations*. Available at <https://www.itu.int/rec/T-REC-K.70-201801-I/en>, last accessed on 26th Feb. 2020.